ACSNANO

www.acsnano.org

ARTICLE

High-Performance Deep Red Colloidal Quantum Well Light-Emitting Diodes Enabled by the Understanding of Charge Dynamics

Sujuan Hu,◆ Farzan Shabani,◆ Baiquan Liu,*,◆ Lingjiao Zhang, Min Guo, Guanhua Lu, Zhisheng Zhou, Jing Wang,* Jacob C. Huang, Yonggang Min, Qifan Xue, Hilmi Volkan Demir,* and Chuan Liu*

Cite This: *ACS Nano* 2022, 16, 10840−10851

Read Online

ACCESS | Metrics & More | Article Recommendations | Supporting Information

ABSTRACT: **Colloidal quantum wells (CQWs) have emerged as a promising family of two-dimensional (2D) optoelectronic materials with outstanding properties, including ultranarrow luminescence emission, nearly unity quantum yield, and large extinction coefficient. However, the performance of CQWs-based light-emitting diodes (CQW-LEDs) is far from satisfactory, particularly for deep red emissions (≥660 nm). Herein, high efficiency, ultra-low-efficiency roll-off, high luminance, and extremely saturated deep red CQW-LEDs are reported. A key feature for the high performance is the understanding of charge dynamics achieved by introducing an efficient electron transport layer, ZnMgO, which enables balanced charge injection, reduced nonradiative channels, and smooth films. The CQW-LEDs based on (CdSe/CdS)@(CdS/CdZnS) ((core/crown)@(colloidal atomic layer deposition shell/hot injection shell)) show an external quantum efficiency of 9.89%, which is a record value for 2D nanocrystal LEDs with deep red emissions. The device also exhibits an ultra-low-efficiency roll-off and a high luminance of 3853 cd m^{-2}. Additionally, an exceptional color purity with the CIE coordinates of (0.719, 0.278) is obtained, indicating that the color gamut covers 102% of the International Telecommunication Union Recommendation BT 2020 (Rec. 2020) standard in the CIE 1931 color space, which is the best for CQW-LEDs. Furthermore, an active-matrix CQW-LED pixel circuit is demonstrated. The findings imply that the understanding of charge dynamics not only enables high-performance CQW-LEDs and can be further applied to other kinds of nanocrystal LEDs but also is beneficial to the development of CQW-LEDs-based display technology and related integrated optoelectronics.**

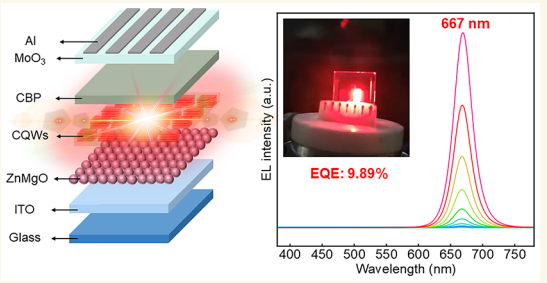

KEYWORDS: *colloidal quantum well, light-emitting diode, charge balance, efficiency, active matrix*

Colloidal quantum wells (CQWs), also known as semiconductor nanoplatelets, are a novel class of optoelectronic materials that have attracted vast attention in the past decade due to their promising properties.[1−8] Owing to the anisotropic shape and one-dimensional quantum confinement along the thickness direction, CQWs demonstrate unique characteristics, including an ultranarrow photoluminescence (PL) signal, a large absorption cross-section, a high exciton binding energy, and a suppressed Auger recombination, which are not easy to achieve in their spherical quantum dot counterparts.[9−15] As a consequence, CQWs have been the subject of extensive studies for optoelectronic technologies, such as lasers, photodetectors, solar energy harvesting, and light-emitting diodes (LEDs), to fully exploit their potential as active materials.[16−21]

As a promising type of nanocrystal LEDs, CQW-LEDs are highly attractive for displays and lighting, because of their outstanding color purity with ultranarrow full-width at half-maximum (fwhm) electroluminescence (EL), feasible solution-processed fabrication, and low power consumption.[22−25] So far, some endeavors have been made to enhance the performance of CQW-LEDs. For example, Sargent et al. used $CdSe_{1-x}S_x$ alloyed core-only CQWs to design LEDs with a peak luminance of ≈100 cd m^{-2}, which is the highest among

Received: March 25, 2022
Accepted: July 5, 2022
Published: July 11, 2022

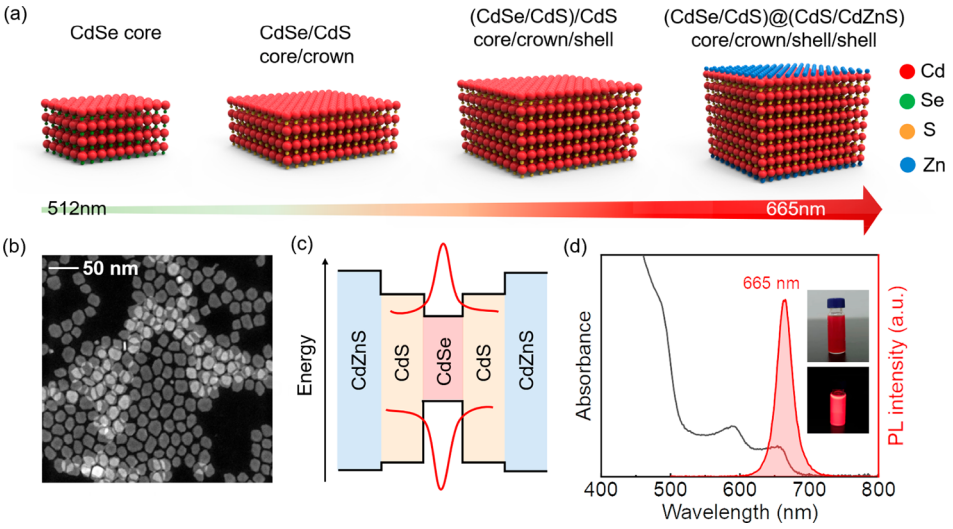

Figure 1. (a) Synthesis pathway of (CdSe/CdS)@(CdS/CdZnS) ((core/crown)@ (c-ALD shell/HIS)) hetero-CQWs. Starting with bare CdSe core, the peripheral sides were first passivated with CdS crown, and then one monolayer of CdS was deposited on the top and bottom side of the CQWs. These CQWs were later used as seeds for the final HIS growth, where CdZnS shell was grown vertically at high temperature. (b) TEM images of CQWs showing maintained 2D shape. (c) Band alignment of CdSe, CdS, and CdZnS. Electrons, with lower effective mass, can easily leak into the CdS shell and contribute to the redshift of the PL, while the outermost layer of CdZnS with high conduction band offset prevent them from reaching to the surface and enhance the PLQY. (d) Absorption and PL spectra of CQWs with electron-heavy hole and electron-light hole peaks distinctly obvious at 654 and 588 nm, respectively, showing that the ensemble is prominently composed of 2D CQWs. Inset: photographs of the CQWs solution under daylight (top) and 365 nm UV light (below).

inverted green CQW-LEDs.[26] Brovelli et al. adopted CdSe/CdZnS core/shell CQWs to construct red LEDs, achieving a peak external quantum efficiency (EQE) of 8.39% and a luminance of ≈100 cd m^{-2}.[27] Ithurria et al. employed halide ligands to release strain in CdSe CQWs, obtaining forward green LEDs with a maximum EQE of <1%.[28] Previously, we also exploited various CQW architectures (e.g., CdSe/$CdSe_{0.8}Te_{0.2}$ core/crown CQWs, Cu-doped CdSe CQWs, and CdSe/CdZnS core/shell CQWs) to develop a series of green, orange, and red LEDs.[29−31] Despite the step-by-step enhancement of CQW-LEDs performance over the past few years, they still lag far behind other kinds of state-of-the-art LEDs (e.g., organic LEDs (OLEDs), colloidal quantum dot LEDs (CQD-LEDs), and perovskite LEDs), particularly for CQW-LEDs with deep red emissions (≥660 nm).[32−40] The low performance may be ascribed to the following factors: (i) CQWs with low PL quantum efficiency (PLQY) are used, which proportionally diminishes the EQE of LEDs. For example, core-only CQWs usually exhibit a low PLQY of <30%.[26,28] (ii) Poor film morphology is formed, which increases the charge leakage and reduces the device stability. For instance, the root-mean-square (R_q) roughness of CQW films is generally >3 nm.[13] (iii) Charge dynamics are not well understood since efficient charge transport layers are rarely reported, which leads to unsatisfactory charge injection, transport, leakage, and balance. To date, only zinc oxide (ZnO) has been identified as effective electron transport layer (ETL) for inverted CQW-LEDs. This may be the reason that the efficiency roll-off is usually serious in CQW-LEDs, restricting the further development of practical applications.[41] Furthermore, although it has been widely anticipated that CQWs are hugely promising for the display technology for more than a decade,[7,8] no active-matrix CQW-LED (AMCQW-LED) has been documented. Therefore, there is a large gap between CQW-LEDs and other types of state-of-the-art LEDs.

Deep red emissions not only make great sense for the next-generation of high-definition color displays with crisp, rich, full color but also meet the requirements of solid-state lighting, especially for high visibility (e.g., optical medical and horticultural lighting) as many photochemical interactions with the human body and chlorophyll have the highest synthesis rate under deep red lighting.[42] Therefore, developing high-performance deep red CQW-LEDs is critical for optoelectronic applications. However, since the human eye has a lower perception of luminance in the spectral range of ≥660 nm, the development of deep red CQW-LEDs is still in its infancy, despite great progress in the performance of green, yellow, orange, and red CQW-LEDs over the past few years. Additionally, the difficulty in the vertical growth of CQWs makes it even harder to extend the emission coverage of CdSe-based CQWs into the deep red wavelengths while maintaining their 2D morphology. As a benchmark, the best EQE of deep red CQW-LEDs is 6.8%, and the highest luminance is 1300 cd m^{-2}.[21] Furthermore, it is not easy to develop extremely saturated red CQW-LEDs. In fact, it is a great challenge to simultaneously obtain high efficiency, low-efficiency roll-off, high luminance, and saturated red emissions, regardless of OLEDs, CQD-LEDs, perovskite LEDs, or CQW-LEDs.[21,40−45]

In this work, we demonstrate high efficiency, ultra-low-efficiency roll-off, high luminance, and extremely saturated deep red CQW-LEDs based on (CdSe/CdS)@(CdS/CdZnS) ((core/crown)@(colloidal atomic layer deposition (c-ALD) shell/hot injection shell (HIS)) CQWs. To achieve high EL performance, an efficient ETL of Mg-doped zinc oxide (ZnMgO) is implemented to enhance the device engineering and better understand the charge dynamics, which is key to achieve balanced charge injection, reduce nonradiative channels, and ensure smooth films. Significantly, the charge dynamics have been comprehensively investigated by both experimental characterizations and technology computer aided design (TCAD) numerical simulation. The resultant CQW-

https://doi.org/10.1021/acsnano.2c02967
ACS Nano 2022, 16, 10840−10851

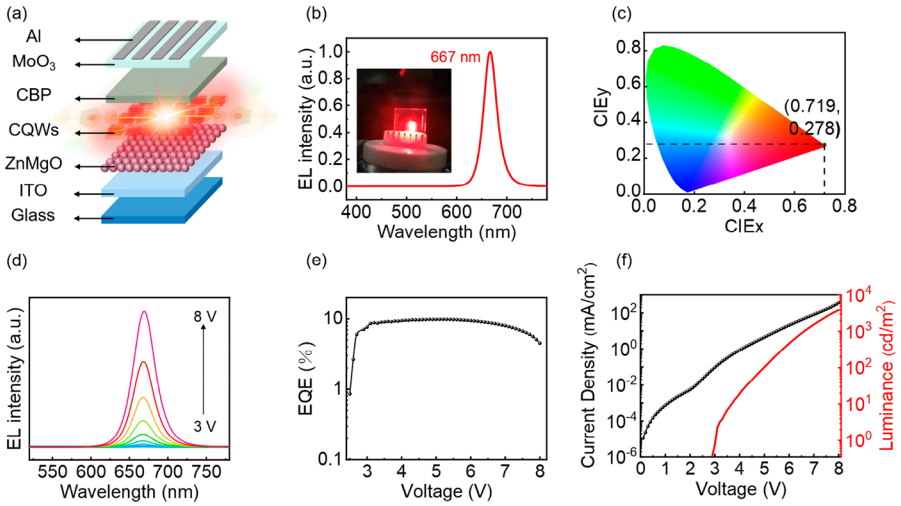

Figure 2. (a) Device structure of CQW-LEDs with ZnMgO as ETL and (CdSe/CdS)@(CdS/CdZnS) ((core/crown)@(c-ALD shell/HIS)) CQWs as the active material. (b) EL spectrum at ~3000 cd m^{-2}. Inset is a photograph of CQW-LEDs under bias. (c) Corresponding coordinates of (0.719, 0.278) in the CIE diagram positioned in the far-red region. (d) EL spectra of CQW-LEDs under different bias, showing no shift with increasing the bias. (e) EQE of Device A versus voltage with the highest EQE of 9.89% at 5.2 V. (f) Current density and luminance of Device A.

LEDs exhibit a maximum EQE of 9.89%, which is not only the best among deep red CQW-LEDs but also a record value for 2D nanocrystal LEDs with deep red emissions, to the best of our knowledge. The device also exhibits an ultra-low-efficiency roll-off and a maximum luminance of 3853 cd m^{-2}. Impressively, an extraordinary color purity, with the Commission Internationale de l'Eclairage (CIE) coordinates of (0.719, 0.278), and highly stable emissions at different voltage are achieved, indicating that the color gamut covers 102% of the International Telecommunication Union Recommendation BT 2020 (Rec. 2020) standard in the CIE 1931 color space, which is the highest reported number for CQW-LEDs. Furthermore, we have demonstrated a prototype AMCQW-LED pixel circuit, through connecting thin film transistor (TFT, an insulated gate field effect transistor that modulates the current between source and drain electrodes through a voltage-charged gate, is usually used to drive pixels in the display field) source terminal with CQW-LEDs.

RESULTS AND DISCUSSION

To achieve efficient deep red CQW emitters, a heterostructure of (CdSe/CdS)@(CdS/CdZnS) ((core/crown)@(c-ALD shell/HIS)) CQWs was designed and synthesized by multiple techniques.[21,46] Figure 1a presents the synthesis process of the hetero-CQWs, where the seeds for the final HIS growth are designed not only to be transversely large and passivated but also to have a relatively large thickness which can be effectively increased by the final HIS coating. Further details of the syntheses can be found in the Supporting Information. Energy-dispersive spectrometry (EDS) (Figure S1) elemental analysis indicates a high percentage of Zn in the CQWs, which together with X-ray photoelectron spectroscopy (XPS) (Figure S2) reveals the successful formation of CdZnS shell. The transmission electron microscopy (TEM) images (Figure 1b) of the CQWs show that the extended emission coverage to the deep red region of the spectra comes with no compromise of the 2D morphology even after multistep shell growth. As discussed before, Cd and Zn atoms tend to reorganize themselves through atomic diffusion, so the strain induced by the lattice mismatch of different domains is minimized.[21] The reorganization of the cations at high temperature forms a Zn-rich shell at the outermost layers of the CQWs with much higher conduction band offset compared to CdSe and CdS (Figure 1c), which prevents the excitons to reach to the surface and effectively enhance the optical properties of the CQWs. The energy band diagram (Figure 1c) of CdSe, CdS, and CdZnS indicates the effectively enhancement of exciton confinement after passivation of the outermost layers of CQWs with CdZnS. The X-ray diffraction (XRD) (Figure S3) pattern of the CQWs shows a typical zinc blende crystalline structure with the (111) planes having the highest diffraction intensity. The position of the original CdSe peaks is shifted toward higher degrees due to the lower lattice constant of ZnS, and as no new peak emerged, the possibility of renucleation or formation different subspecies is diminished. Together with the red-shifted absorption and emission spectra, these measurements demonstrate an effective enhancement of the thickness of the CQWs in which CdZnS shell is deposited through the final HIS coating and yields very thick CQWs emitting in the deep red (665 nm) region of the spectra, as shown in Figure 1d. These CQWs possess exceptionally high chemical stability that even after 5 cycles of cleaning no obvious precipitation was observed and the in-solution PLQY remained as high as 81%, which further emphasizes the potency of the hybrid inorganic/organic surface passivation of the CQWs by CdZnS shell and organic ligands.[34]

To understand the EL properties of the CQWs, we fabricated CQW-LEDs with the inverted hybrid organic–inorganic architecture (Device A, Figure 2a) with a structure of indium tin oxide (ITO, 115 nm)/ZnMgO (30 nm)/CQWs (35 nm)/4,4-*N*,*N*-dicarbazolebiphenyl (CBP, 40 nm)/molybdenum trioxide (MoO_3, 6 nm)/Al (80 nm), where ITO and Al function as cathode and anode, respectively. ZnMgO is used as the ETL (the Mg content of ZnMgO nanoparticles is optimized to be 15.0 mol %, i.e., $Zn_{0.85}Mg_{0.15}O$), and CQWs are used as the emitting layer (EML). CBP and MoO_3 serve as the hole-transporting layer (HTL) and hole-injecting layer (HIL), respectively. A cross-sectional scanning electron

https://doi.org/10.1021/acsnano.2c02967
ACS Nano 2022, 16, 10840–10851

microscopy (SEM) image of Device A is presented in Figure S4.

Previously, the efficiency of ZnO nanocrystals as ETL was found to be higher than other materials for inverted CQW-LEDs. However, ZnO ETL tends to inject an excess of electrons due to incompatibility with the low hole mobility and injection rate of the HTLs, resulting in weak charge balance.[47] For CQW-LEDs with the combination of CBP HTL and ZnO ETL, since the hole mobility of CBP (1×10^{-3} cm^2 V^{-1} s^{-1})[23] is lower than the electron mobility of ZnO (1.8×10^{-3} cm^2 V^{-1} s^{-1}),[31] superfluous electrons will be injected into the EML, leading to the increased nonradiative Auger recombination. Despite a lack of thorough investigation in the literature to address this problem, ETLs are required to be engineered for an effective charge injection and balance. Herein, we explored ZnMgO nanocrystals as a possible candidate for ETL in CQW-LEDs since ZnMgO is expected to increase the resistivity compared to ZnO and mitigate excessive electrons in organic–inorganic hybrid LEDs, which leads to a more balanced charge injection.[48,49]

As shown in Figure 2b,c, the EL emission peak wavelength of CQW-LEDs is located at 667 nm, corresponding to the CIE coordinates of (0.719, 0.278). To meet the demand of the Rec. 2020 standard for next-generation ultra-high-definition TVs, extremely saturated red emissions are required.[50] The color gamut of Device A covers 102% of the Rec. 2020 standard in the CIE 1931 color space, which is the highest for CQW-LEDs, indicating that CQW-LEDs have a huge potential for the display technologies. The photograph displayed in the inset of Figure 2b shows a bright deep red color from a working CQW-LED with a luminance of ∼3000 cd m^{-2}, indicating successful realization of deep red CQW-LEDs in our study. Additionally, stable colors are needed for the practical display and lighting applications. As exhibited in Figure 2d, the EL peak wavelength remains in its place and does not change in position with increasing voltages. Moreover, there is no emission generated from neighboring charge transport layers, implying that electrons and holes are well recombined at CQW emitters.

The maximum EQE of Device A is 9.89% (Figure 2e and Table 1), which is not only the highest for deep red CQW-LEDs but also a record value for 2D nanocrystal LEDs with deep red emissions. In addition, the efficiency roll-off, a significant parameter of LEDs for practical applications, is well-resolved in our device. The critical current density j_c, where EQE declines by half from its peak,[51] is as high as ∼320 mA cm^{-2} (the maximum EQE is obtained at 6.2 mA cm^{-2}). The EQE$_{80}$ (defined as the EQE possessing 80% of the maximum value) ranged from a low voltage of 3.1 V to a high voltage of 7.0 V, which covers 80% of the whole working voltages. At the display-related luminance of 100 cd m^{-2}, the EQE is 9.86%. Even at the lighting-related luminance of 1000 cd m^{-2}, the EQE remains as high as 8.35%. Therefore, an ultra-low-efficiency roll-off is achieved. The results indicate that Device A exhibits a good charge balance, since the efficiency roll-off is generally caused by either luminescence quenching (i.e., a reduction in luminescence efficiency due to nonradiative processes or an excessive population of charge carriers passing through the device without forming electron–hole pairs).[41] The maximum luminance of Device A is 3853 cd m^{-2} (Figure 2f), which is nearly 3 times higher than that of the previous best deep red CQW-LEDs.[21,30] Therefore, our CQW-LEDs can simultaneously obtain high efficiency, ultra-low-efficiency roll-off, high luminance, stable color, and extremely saturated red emissions, which was not possible for previous nanocrystal LEDs.

Table 1. Summary of the Performance of CQW-LEDs

Device	PLQY[a]	λ_E (nm)[b]	V_{on} (V)[c]	EQE$_{max}$ (%)[d]	FWHM (nm)[e]
A (ZnMgO)	81%	667	2.9	9.89	30
B (ZnO_a)	81%	667	2.4	8.89	30
C (ZnO_b)	81%	669	2.5	3.47	32
D (In_2O_3)	81%	668	3.2	4.47	33

[a]PLQY of CQW emitters in hexane. [b]EL emission peak. [c]Turn-on voltage (the voltage when the luminance is >0.1 cd m^{-2}); [d]Maximum EQE; [e]FWHM of CQW-LEDs.

To understand the origin of the high performance of Device A, the effect of charge dynamics in CQW-LEDs should be unveiled. Therefore, we comprehensively investigated charge injection, charge transport, charge recombination, and charge leakage. Since CQWs are solution-processed on the top of ZnMgO, the ETL plays a crucial role in the performance of CQW-LEDs. To reveal the influence of ETLs in CQW-LEDs, three more ETLs with different compositions or solvents have been examined: (i) ZnO nanocrystals synthesized via easy in-solution process in ambient temperature and without need of any specific condition (designated as ZnO_a) for Device B. (ii) ZnO nanoparticles dissolved in ammonium hydroxide (50% v/v) solution (designated as ZnO_b) for Device C. (iii) Indium oxide (In_2O_3) nanocrystals synthesized via indium(III) nitrate hydrate dissolved in water for Device D. The device structure of all these CQW-LEDs remained the same as that of Device A with general architecture of ITO/ETLs (30 nm)/CQWs/CBP/MoO_3/Al, and only the ETL is altered accordingly. ZnO is selected since it is an intensely studied ETL for CQW-LEDs, which is beneficial to understand the charge dynamics with the comparison of ZnO and ZnMgO. Additionally, we have investigated In_2O_3 as ETL since it is an ideal semiconductor material for optoelectronics due to the high mobility and charge concentration,[52,53] despite no report of its performance in CQW-LEDs.

To better understand the effect of ETLs, the performance of Devices A–D has been systematically compared. As shown in Figure 3 and Table 1, the EL spectra of Devices B–D are almost similar to that of Device A. However, the maximum EQE of Device B (8.89%), Device C (3.47%), and Device D (4.47%) is much lower than that of Device A. Additionally, it is clearly seen that the efficiency roll-off in Devices B–D is much higher than that of Device A. Therefore, the highest EQE and the lowest efficiency roll-off of Device A can be attributed to the selection of ZnMgO as ETL, since all other layers in these CQW-LEDs are similar except for the ETL. These results conclusively suggest that ZnMgO is the best ETL of the four ETLs to guarantee the device efficiency.

The origin of the best EQE and minimized efficiency roll-off achieved by Device A can be explained as follows. In LEDs, the EQE is usually defined as[54]

$$\mathrm{EQE} = f_{\mathrm{balance}} \cdot \gamma_{\mathrm{st}} \cdot q \cdot \eta_{\mathrm{out}} \quad (1)$$

where f_{balance} represents the charge balance factor, γ_{st} is the fraction of excitons that radiatively decay, q is the PLQY of emitters, and η_{out} is the outcoupling factor. As the LED is an injection-type device, electrons and holes are expected to be

https://doi.org/10.1021/acsnano.2c02967
ACS Nano 2022, 16, 10840–10851

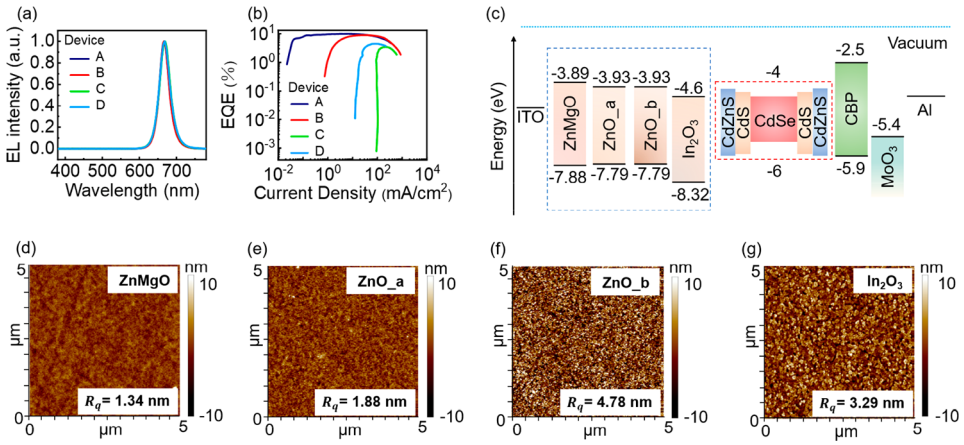

Figure 3. (a) EL spectra of CQW-LEDs with different ETLs of ZnMgO, ZnO (in ethanol), ZnO in ammonium hydroxide (50% *v*/*v*), and In_2O_3, designated as Devices A−D, respectively. (b) EQEs of different ETLs-based CQW-LEDs. (c) Schematic flat-band energy diagram of CQW-LEDs. AFM images for ZnMgO film (d), ZnO_a film (e), ZnO_b film (f), and In_2O_3 film (g).

injected from two end electrodes. However, the balanced number of electrons and holes arrived at the EML may be disturbed due to their passage through different transmission layers, which ultimately alters $f_{balance}$. Hence, as $f_{balance}$ gets closer to 1, a more balanced injection of electrons and holes in the device is guaranteed. For γ_{st} and q, the theoretical limit value for CQWs is 100%, which can be achieved through adjusting the surface ligands and synthesis protocol, and it is an intrinsic property of the emitting material that is not related to the device design. For η_{out}, due to the absorption and reflection of ITO substrate, electrodes materials, and other layers in the device, the optical coupling efficiency of common ITO glass substrate is about 20%. Therefore, as η_{out} is not affected by the internal operation, and γ_{st} and q are dictated by the nature of the emitting material, the EQE of CQW-LEDs is mainly determined by $f_{balance}$ according to eq 1.

First, the charge mobility has an influence on $f_{balance}$. The electron mobility of ZnO and In_2O_3 is much higher than the hole mobility of CBP, which indicates that electrons and holes are easily unbalanced in Devices B−D, leading to the poor device performance. However, the relatively low electron mobility of ZnMgO avoids excess electrons, ensuring more balanced charges. These analyses are confirmed by the current density of Devices A−D (Figure S5), since Device A exhibits the lowest current density due to the reduced electron mobility of ZnMgO. To further demonstrate the fact that ZnMgO can lower the electron transport for a better charge balance, electron-only devices have been fabricated with the structure of ITO/ETLs/CQWs/2,2′,2″-(1,3,5-benzenetriyl) tris-[1-phenyl-1*H*-benzimi dazole] (TPBi)/LiF/Al, where the ETLs are ZnMgO, ZnO_a, ZnO_b, and In_2O_3. As shown in Figure S6, the ZnMgO-based electron-only device possesses the lowest current density, which is consistent with the phenomena in the fabricated CQW-LEDs, indicating that ZnMgO can effectively avert the excess electrons. As further evidence on true charge balance $f_{balance}$, a hole-only device with the structure of ITO/CQWs/CBP/MoO_3/Al and a simple electron-only device with structure of ITO/ZnO_a/CQWs/Al are produced, which are split from the device structure of Device B. As show in Figure S7, the electron current of the electron-only device is much larger than the hole current of the hole-only device, which qualitatively demonstrates the fact that excess electrons exist in ZnO-based CQW-LEDs, leading to the weak charge balance. Hence, the balanced charges in Device A guarantee the high performance.

In addition to the charge mobility, the energy barrier is another factor to greatly affect the charge transport. Through the ultraviolet photoelectron spectroscopy (UPS) characterization (Figure S8) and extraction of relevant parameters,[49,55] the energy band diagram of the devices was calculated and presented as a flat-band schematic in Figure 3c. Electrons are free from barriers to reach CQWs from ETLs in Devices A−C, since the conduction band minimums (CBM) of ZnMgO (3.89 eV) and ZnO (3.93 eV) are shallower than that of CQWs (~4 eV). In addition, it is noted that although electron injection is sub-Ohmic at the ETL/CQW interfaces of Devices A−C, the CBM offset introduces a higher electron barrier at the ITO cathode in Device A since the CBM of ZnMgO (3.89 eV) is about 40 meV above that of ZnO (3.93 eV), which is also responsible for the higher V_{on} (2.9 V) and better charge balance. However, electrons are difficult to arrive at CQWs in Device D due to the large barrier (~0.6 eV) between the CBM of In_2O_3 and CQWs. In contrast, the hole barrier between CQWs and CBP is small (0.1 eV). Therefore, from the perspective of energy barrier at the interface of CQWs and charge transport lays, both electrons and holes are readily located at CQWs in Devices A−C, while only holes are feasibly transported to CQWs in Device D. Considering the high electron mobility and large electron barrier between In_2O_3 and CQWs, electrons are easily accumulated at the interface of In_2O_3 and CQWs, which causes a narrow charge recombination zone. As a result, exciton quenching will easily occur, which is another reason for the poor performance of Device D.

For solution-processed LEDs, the film morphology of the active layer has an important effect on the device performance. Hence, the EQE of solution-processed LEDs (EQE′) can be written as

$$EQE' = \alpha \cdot f_{balance} \cdot \gamma_{st} \cdot q \cdot \eta_{out} \quad (2)$$

where α represents the factor of film morphology, emphasizing the significance of film roughness on the leakage current. The value of α is assumed to be ≤1 and proportional to the roughness of films.[31] The surface roughness of ETL films were measured by atomic force microscopy (AFM). The R_q of ZnMgO film is 1.34 nm (Figure 3d), which is much smoother than those of ZnO_a (1.88 nm, Figure 3e), ZnO_b (4.78 nm,

https://doi.org/10.1021/acsnano.2c02967
ACS Nano 2022, 16, 10840−10851

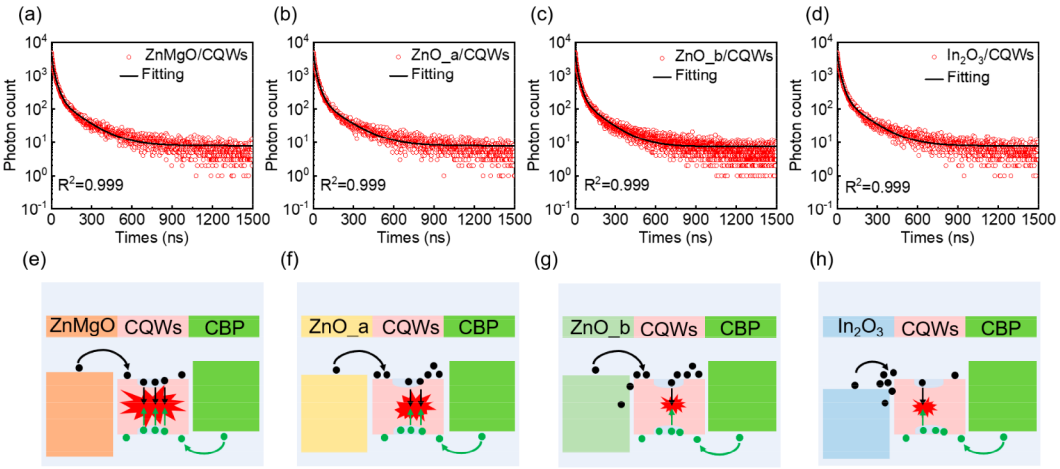

Figure 4. TRPL analyses of CQWs on ZnMgO film (a), ZnO_a film (b), ZnO_b film. (c), and In_2O_3 film (d). Charge dynamics mechanism of Device A (e), Device B (f), Device C (g), and Device D (h). Black and green solid circles represent electrons and holes, respectively.

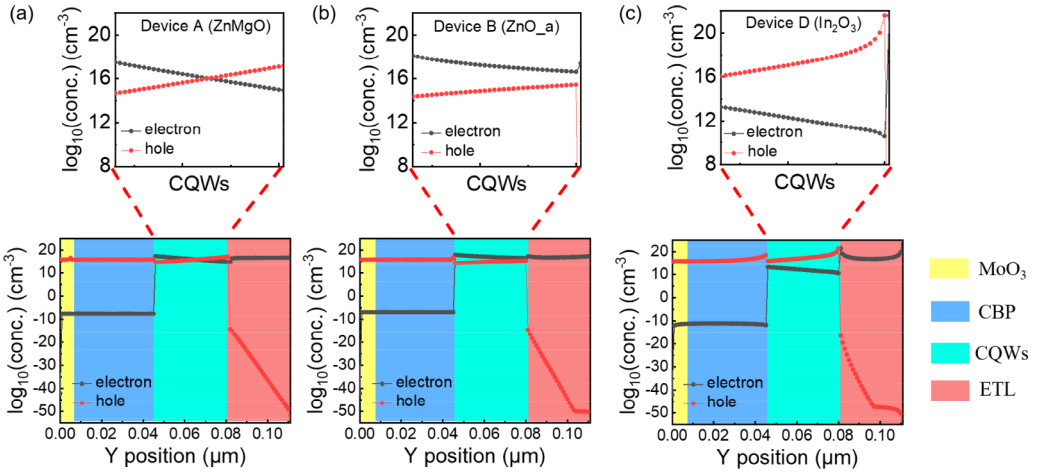

Figure 5. Distributions of electrons and holes in the vertical direction of Device A (a), Device B (b), and Device D (c) at V_{anode} = 6 V and $V_{cathode}$ = 0 V.

Figure 3f), and In_2O_3 (3.29 nm, Figure 3g). Therefore, in Device A, the possibility of a morphologically induced electrical short and charge leakage are significantly reduced, leading to the high device performance.[31] Particularly, the film roughnesses of Devices C and D are very high, which easily causes a large leakage current and induces a mass of defect recombination and Auger recombination. This is an important reason for the fact that the current density of Devices C and D is very high at low voltages, while the peak luminance (e.g., 1848 cd m^{-2} for Device D) is very low (Figure S9).

In addition, ETLs can induce the exciton quenching on the PL and EL emissions of CQWs,[29] which is detrimental to the device performance. The average PL lifetime (τ_{ave}) of CQWs on ZnMgO film is 59.6 ns (Figure 4a), which is better than that of CQWs on ZnO_a film (58.9 ns, Figure 4b), ZnO_b (53.6 ns, Figure 4c), and In_2O_3 film (57.4 ns, Figure 4d). The detailed analyses of τ_{ave} are shown in Table S1. Considering that the difference in lifetime is small, there may be almost no effect on the CQW dynamics in all cases. This phenomenon makes sense as it is known that the exciton quenching by ZnO is due to electron injection from ZnO to the CBM of CQWs, leading to charging and Auger decay. Since all ETLs except In_2O_3 have a higher CBM than CQWs, such an effect may occur in all systems, or in none if, for instance, the ligand barrier prevents the transfer.

From the above facts, we can establish the charge dynamics mechanism of the four fabricated CQW-LEDs. For Device A, because of its good surface morphology, suitable charge injection, and charge transfer capability, the electrons injected into CQWs are in the closest balance with the holes injected into CQWs by CBP (Figure 4e). Therefore, Device A simultaneously has high EQE, minimized efficiency roll-off, and high luminance. For Device B, due to the relatively high electron injection and transport, excessive electron injection occurs, leading to the relatively lower charge balance together with the fact that the recombination position is biased to the CBP side (Figure 4f). In addition, the surface morphology of ZnO_a is worse than that of ZnMgO, inducing a certain leakage current and further intensifying the unwanted of nonradiative recombination. Therefore, the EQE of Device B is lower than that of Device A. For Device C (Figure 4g), the solvent of ZnO_b has a certain exciton quenching effect on CQWs and a rough film, which causes a large charge leakage. Additionally, ZnO_b has a relatively high electron injection and transport. All these factors lead to the recombination position being further biased to the side of the HTL, resulting in defect recombination and Auger recombination. For Device

https://doi.org/10.1021/acsnano.2c02967
ACS Nano 2022, 16, 10840−10851

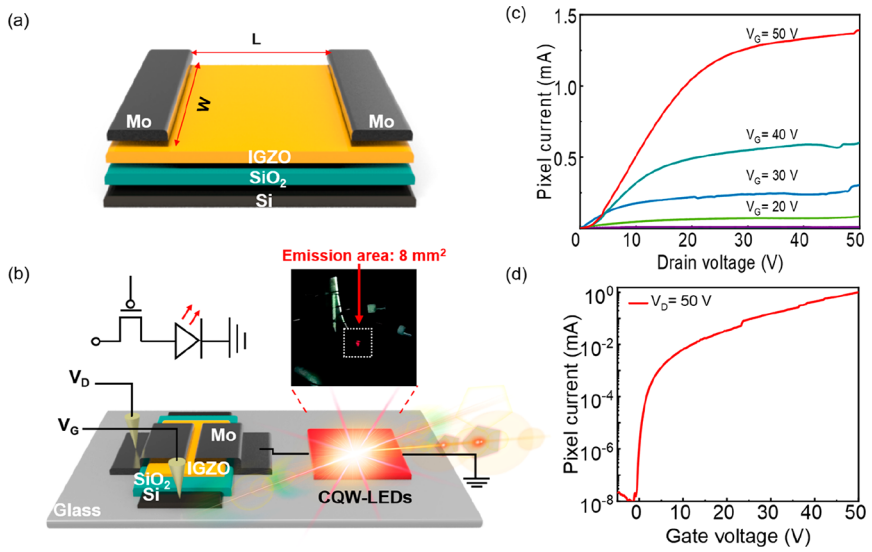

Figure 6. (a) Device structure of TFTs. The gate insulator is 100 nm. The IGZO channel layer is ~50 nm, and the width (W) and length (L) of the channel are 750 and 350 μm, respectively. (b) Diagram of the AMCQW-LED pixel circuit and test. The emission area is 8 mm^2. (c) Output curves of the AMCQW-LED pixel circuit (V_G scans from 0 to 50 V in a step of 10 V). (d) Transfer curves of the AMCQW-LED pixel circuit (V_D = 50 V).

D (Figure 4g), owing to the mismatched energy barrier between In_2O_3 and CQWs, it is difficult for electrons to be injected into CQWs. This leads to a mass of electrons accumulating at the In_2O_3/EML interface and shift the recombination position to the In_2O_3/EML interface. Furthermore, the rough morphology of the film also causes a large charge leakage, which can easily induce nonradiative recombination, leading to a poor performance.

According to the above analyses, for the four ETLs-based CQW-LEDs, $f_{balance}$ may have the following relationship:

$$1 \geq f_{balance}(A) > f_{balance}(B) > f_{balance}(D) > f_{balance}(C) \quad (3)$$

Therefore, the relationship of EQE for CQW-LEDs can be written as

$$\mathrm{EQE(Device\ A)} > \mathrm{EQE(Device\ B)} > \mathrm{EQE(Device\ D)} > \mathrm{EQE(Device\ C)} \quad (4)$$

In particular, the EQE of Device A (9.89%) is 285% higher than that of Device C (3.47%), indicating that the understanding of charge dynamics is believed to be an alternative route to improve the performance of CQW-LEDs.

The above analyses are further supported by more detailed optoelectronic device modeling where the characteristic electrical simulators of the parameters of ETLs (e.g., conduction bands, valence bands, mobility, and conductivity) are performed using a 2D device tool (Atlas, Silvaco TCAD). We explored the mechanism of charge injection and balance and studied the distribution of charge concentration, energy band, potential, and recombination rate. The simulation structures are shown in Figure S10, and the specific material parameters are summarized in Table S2. The distributions of electrons and holes in the vertical direction of Devices A, B, and D at the anode voltage (V_{anode}) of 6 V and the cathode voltage ($V_{cathode}$) of 0 V are shown in Figure 5a–c. Additionally, since the process parameters (e.g., energy level and moblity) of ZnO_a and ZnO_b are basically the same, the simulation of Device C is the same as that of Device B.

In Device A (Figure 5a), the electron concentration in CQWs is close to the hole concentration because of the slightly low mobility, low conductivity, and high band gap of ZnMgO compared to the properties of ZnO_a. Therefore, the electron injection and transport capability of ZnMgO are effectively reduced, and the number of electrons transported to CQWs is in close balance with the number of holes injected through CBP. Additionally, we extracted the energy band, potential, and recombination rate distribution of CQW-LEDs in the vertical direction at V_{anode} = 6 V and $V_{cathode}$ = 0 V (Figure S11). As seen from the potential distribution in Figure S11d,e, the potential drop for ZnMgO is greater than that of ZnO_a, which indicates that the electron injection of ZnMgO is effectively reduced. Furthermore, the recombination rate distribution in CQWs (Figure S11g,h) further confirms that the electron injection of ZnMgO and the hole injection of CBP are more balanced and that electrons and holes are well-recombined at CQW emitters.

In Device B (Figure 5b), the electron concentration in CQWs is higher than the hole concentration. Since the electron mobility of ZnO_a is relatively high and the conduction band of ZnO_a is almost the same as that of the CQWs, this indicates that the electrons can be easily transported from ZnO_a to the CQWs, which can also be explained by the small potential drop on ZnO_a in the CQW-LEDs (Figure S11e). In addition, the hole mobility of CBP is lower than the electron mobility of ZnO_a. These factors can lead to excess electron injection into the CQWs. From Figure S11h, it can be found that ZnO_a has a high recombination rate on the side of CQWs layer closer to the HTL due to its high electron injection and fast electron transport. The offset of recombination position and excessive electron injection can easily induce nonradiative recombination, deteriorating the device performance.

In Device D (Figure 5c), the electron concentration in CQWs is significantly lower than the hole concentration, although In_2O_3 has the highest electron mobility (1.1 cm^2 V^{-1} s^{-1})[55] among all our ETLs and strong hole-blocking ability due to its valence band maximum of 8.32 eV. However, the CBM

https://doi.org/10.1021/acsnano.2c02967
ACS Nano 2022, 16, 10840–10851

of In_2O_3 is very deep (4.6 eV), leading to a large energy barrier (~0.6 eV) between the CQWs and In_2O_3, which is unfavorable for the electron transport, resulting in the large accumulation of electrons at the In_2O_3/EML interface. This electron accumulation can easily result in CQWs charging, which is detrimental to the device performance since such charging can lead to the CQWs luminescence quenching via the non-radiative Auger recombination. Figure S11f shows a large potential drop on In_2O_3 causing the energy band of In_2O_3 to be pulled up (Figure S11c). Therefore, these simulations can support our findings and are beneficial to give a further insightful understanding of charge dynamics.

Finally, it is notable that the outcoupling efficiency is not actually 20% in all cases, considering that this efficiency can be affected by several factors, such as the film roughness, microcavity effect, light absorption, and excited metal surface plasmon resonance. For example, a poor film roughness might increase the outcoupling efficiency and artificially enhance the EQE of the "bad" devices. As a result, it is possible that the effect of ZnMgO might, in fact, be bigger than expected. Hence, the understanding of the outcoupling mechanism in CQW-LEDs may require a further systematical study. Additionally, it is noted that ZnMgO-based CQW-LEDs can exhibit a lifetime of 11.9 h at 100 cd m^{-2} (Figure S12), which is the best for CQW-LEDs without encapsulation. The stability of CQW-LEDs may be further improved if more stable hole transport materials (e.g., appropriate inorganic materials), more stable CQWs (e.g., CQWs are not negatively influenced by oxygen and humidity), and advanced encapsulation technology were used.

Currently, active-matrix displays are considered as the mainstream display technology.[56] In fact, active-matrix OLEDs (AMOLEDs)[57] and active-matrix CQD-LEDs[58] have been reported for more than 10 years. However, so far there has been no realization of AMCQW-LEDs. To loosen this bottleneck and encouraged by our high-performance CQW-LEDs, we have further integrated CQW-LEDs with TFTs. To realize the concept of AMCQW-LEDs, *n*-channel TFTs are selected because of the compatibility of the bottom electron injection electrode inverted architectures with *n*-channel TFTs. Therefore, indium gallium zinc oxide (IGZO) with stable performance and mature preparation technology is used as the active layer to construct n-type TFT,[59−61] which can adjust the current to drive CQW-LEDs by choosing the suitable length and width of the channel. The TFT structure is shown in Figure 6a. We constructed AMCQW-LEDs by connecting the *n*-channel TFT source electrode with CQW-LEDs (Figures 6b and S13). As shown in Figure 6c,d, the pixel current of the CQW-LEDs could be modulated in a wide range by scanning the gate voltage (V_G) from 0 to 50 V, and the light emission intensity of CQW-LEDs is also modulated as the current density changes (Figure S14). Thus, our AMCQW-LEDs demonstrate high control capability, proving the feasibility of CQW-LEDs as a potential kind of LEDs for the display technology.

CONCLUSION

To conclude, high-performance deep red CQW-LEDs based on (CdSe/CdS)@(CdS/CdZnS) ((core/crown)@(c-ALD shell/HIS)) hetero-CQWs have been achieved, which can simultaneously exhibit high efficiency (EQE = 9.89%), ultra-low-efficiency roll-off, high luminance (3853 cd m^{-2}), and extremely saturated deep red emission with the color gamut covering 102% of the Rec. 2020 standard. ZnMgO is found to be an excellent ETL for CQW-LEDs, which enables balanced charge injection, reduced nonradiative channels, and smooth film formation. Importantly, charge dynamics have been thoroughly investigated by both experimental characterizations and TCAD numerical simulation, which unveils the origin of the high device performance. AMCQW-LEDs have been realized by connecting an IGZO-based TFTs source electrode with CQW-LEDs. The results indicate that the understanding of charge dynamics not only enables high-performance CQW-LEDs and can be further applied to other kinds of nanocrystal LEDs but also is a huge step forward toward the CQW-LEDs based display technology and related integrated optoelectronics.

METHODS

Chemicals. Cadmium acetate dihydrate ($Cd(Ac)_2·2H_2O$, 98%), cadmium acetate ($Cd(Ac)_2$, 99.995%), cadmium nitrate tetrahydrate ($Cd(NO_3)_2·4H_2O$, ≥99.0%), zinc acetate dihydrate ($Zn(Ac)_2·2H_2O$, 98%), zinc acetate ($Zn(Ac)_2$, 99.99%), cadmium nitrate, sodium myristate (≥99.0%), selenium (99.99%), 1-octanethiol (≥98.5%), sulfur (99.98%), ammonium sulfide solution ($(NH_4)_2S$, 40−48 wt % in H_2O), oleic acid (OA, 90%), oleylamine (OLA, 70%), 1-octadecene (ODE, 90%), ethanol (absolute), methanol (≥99.7%), *N*-methylformamide (NMF, 99%), *n*-hexane (≥97.0%), toluene (≥99.5%), acetonitrile (≥99.9%), ZnO nanoparticles (nanopowder, <50 nm particle size (BET), >97%), indium(III) nitrate hydrate (99.9%), tetramethylammonium hydroxide (TMAH, 98%), ethyl acetate (99.9%), dimethyl sulfoxide (DMSO, ≥99.9%), ethanolamine (≥99.9%), and water deionized were obtained from Sigma-Aldrich. 4,4-*N*,*N*-Dicarbazolebiphenyl (CBP) was purchased from Xi'an Polymer Light Technology Corp. 1,3,5-Tris(1-phenyl-1*H*-benzimidazole-2-yl)benzene (TPBi) was purchased from Lumtec. Ammonium hydroxide (50% *v*/*v*) solution was purchased from Alfa Aesar. All chemicals were used as received.

Cadmium Myristate Synthesis. Cadmium myristate ($Cd(myr)_2$) synthesis was adopted from the literature, with no modification.[20] Cadmium nitrate (1.23 g) was dissolved in 40 mL of methanol, and 3.13 g of sodium myristate was dissolved in 250 mL of methanol (1 h with strong stirring). After complete dissolution, the two solutions were mixed, giving a white precipitate. This precipitate was filtered and washed on a Buchner vacuum flask and dried under vacuum for about 12 h.

Synthesis of CdSe Core. CdSe core CQWs (4 ML) were synthesized according to the recipe in the literature, with no modification.[20]

Synthesis of CdSe/CdS Core/Crown CQWs. CdSe/CdS core/crown CQWs (4 ML) were synthesized according to the literature, with slight modifications.[20] In the first step, the crown solution precursor was made by mixing of 2.4 g of $Cd(Ac)_2·2H_2O$, 1.7 mL of OA, and 10 mL of ODE. The mixture was alternatively stirred at 150 °C and sonicated at 100 °C, until a homogeneous white solution was obtained. In a typical synthesis of 4 ML CdSe/CdS core/crown CQWs, 4 mL of 4 ML CdSe core CQWs (optical density (OD) of 1 at wavelength of 350 nm when 100 μL of the core solution was mixed in 3 mL of hexane), was mixed with ethanol and centrifuged. The precipitate was redispersed in 1 mL of hexane, and the solution was put in a 50 mL three-neck flask alongside with 400 μL of OA and 20 mL of ODE. The solution was kept under vacuum at 90 °C for 1 h to remove the water and other volatile species. Then, under argon gas, a mixture of 400 mL of S-ODE (0.1 M) and 2.4 mL of crown solution was injected into the flask, and the temperature was set to 225 °C. When the temperature reached to 225 °C, the flask was quenched in a water bath. The CQWs were collected and diluted with 15 mL of hexane, and then centrifuged at 6000 rpm for 6 min. The supernatant was mixed with ethanol and centrifuged at 6000 rpm for 6 min to precipitate the core/crown CQWs. Finally, 4 ML CdSe/CdS core/crown CQWs were dispersed in hexane and kept for further use.

https://doi.org/10.1021/acsnano.2c02967
ACS Nano 2022, 16, 10840−10851

Synthesis of (CdSe/CdS)@(CdS) (core/crown)@(c-ALD shell) CQWs. The c-ALD shell coating of the CQWs has been done according to the literature with minor modification.[46] First, the previously synthesized 4 ML CdSe/CdS core/crown CQWs were precipitated through addition of ethanol and centrifugation and redispersed in hexane for a total of 6 times to remove the unreacted chemicals from previous synthesis steps. Then, 1 mL of NMF was added to 1 mL of the solution of the CQWs, and 75 μL of ammonium sulfide was added to the biphasic solution. The solution was stirred for 3 min to cover the outer layers of CQWs with sulfur, which caused the CQWs to transfer from hexane to NMF. Hexane was removed with a pipet, and the CQWs were precipitated from NMF by addition of acetonitrile and toluene and centrifugation. The CQWs were precipitated/redispersed in NMF 2 times to remove the unreacted ammonium sulfide. The Cd layer was deposited on the CQWs by addition of 2 mL of $Cd(NO_3)_2{\cdot}4H_2O$–NMF (1 M) to the solution, and stirring for 15 min. The CQWs were precipitated/redispersed 6 times, and the last precipitate was transferred to hexane by addition of 2 mL of OLA at 50 °C and stirring for 2 min. The final CQWs were kept in hexane for the final hot-injection shell growth step.

Synthesis of (CdSe/CdS)@(CdS/CdZnS) ((core/crown)@(c-ALD shell/HIS)) CQWs. The final hot-injection shell coating has been done according to the published recipe in the literature with some modifications.[23] In a typical synthesis, the (CdSe/CdS)@CdS (core/crown)@(c-ALD shell) CQWs capped with OLA were mixed with 3.5 mL of ODE, 500 μL of OA, 0.15 mmol of $Zn(Ac)_2$, and 0.05 mmol of $Cd(Ac)_2$ in a 50 mL three-necked flask, and the solution was degassed at room temperature for 1.5 h, then further degassed at 80 °C for 30 min. Then, the flask was flushed with argon gas, and 500 μL of OLA was added to the solution. After that, the temperature was set to 300 °C, and before it reaches 165 °C, an anion precursor of octanethiol–ODE (0.1 M) was added to the solution with an injection rate of 10 mL h^{-1}. For the temperatures above 240 °C, the injection rate was decreased to 4 mL h^{-1}. The flask was kept at a high temperature of 300 °C for 60–120 min, and then it was quenched via water bath. Then, the solution was collected and diluted with 5 mL of hexane. The unstable particles were precipitated out by centrifugation at 6000 rpm for 6 min. The final CQWs were separated by addition of ethanol and centrifugation, and they were kept in hexane.

ZnO Synthesis. The ZnO ethanol solution was synthesized according to the literature, with slight modifications.[47] First, 3 mmol of $Zn(Ac)_2{\cdot}2H_2O$ was dissolved in 30 mL of DMSO. Then, 5.5 mmol of TMAH was dissolved in 10 mL of ethanol and stirred for 10 min at 50 °C in a water bath. The TMAH solution was added to the $Zn(Ac)_2$ solution and stirred for 2 h at 50 °C in a water bath. Then, the solution was collected and diluted with ethyl acetate and centrifuged at 5000 rpm for 3 min. The ZnO nanoparticles were dispersed in ethanol. The ZnO nanoparticles were precipitated/redispersed for 2 times.

ZnMgO Synthesis. ZnMgO was synthesized according to the literature with slight modifications.[62] First, 2.55 mmol of $Zn(Ac)_2{\cdot}2H_2O$ and 0.45 mmol $Mg(Ac)_2{\cdot}4H_2O$ were dissolved in 30 mL of DMSO and stirred for 10 min at 50 °C in a water bath. Separately, 5 mmol of TMAH was dissolved in 10 mL of ethanol and stirred until dissolved. The TMAH solution was added to the $Zn(Ac)_2$ and $Mg(Ac)_2$ mixture solution with an injection rate of 40 mL h^{-1}, and after the injection was complete, it was kept stirring for 1 h at 50 °C in a water bath. Then, the solution was collected and diluted with ethyl acetate and centrifuged at 5000 rpm for 3 min. The ZnMgO nanoparticles were dispersed in ethanol. The ZnMgO nanoparticles were precipitated/redispersed 2 times.

CQW-LEDs Device Fabrication. CQW-LEDs were fabricated on a patterned ITO-coated glass substrate, which was cleaned by sonication in detergent, acetone, isopropyl alcohol, and deionized water, then dried in an oven with 65 °C. After 4 min of oxygen plasma treatment of the ITO to prepare a clean and hydrophilic surface, the electron transfer layer (ETL) precursor solution was spin-coated on the ITO substrate at 3000 rpm for 45 s and baked at 150 °C for 10 min in a N_2-filled glovebox. CQWs precursor solution was then spin-coated on top of the ETL film at 2000 rpm for 40 s in a N_2-filled glovebox. Finally, CBP (60 nm), MoO_3(6 nm), and Al electrodes (100 nm) were deposited under high-vacuum conditions of $<1 \times 10^{-6}$ Torr. The active area of the device was 8 mm^2, defined as the overlapping area of the cathode and anode electrodes.

TFT Device Fabrication. The TFT device was fabricated on a 100 nm thermally oxidized SiO_2/Si substrate. The a-IGZO channel layer was ∼50 nm thick and deposited by pulsed laser deposition with a KrF excimer laser (∼248 nm) at room temperature. Oxygen partial pressure was fixed at P_{O_2} = 2.5 Pa during the deposition. The distance between the $InGaZnO_4$ target and substrate was 4.5 cm. After deposition, the sample was annealed at 350 °C for 1 h in air atmosphere. Then, the source and drain electrodes areas were fabricated by photolithography and lift-off processes. The electrodes were formed by sequential deposition of Mo layer using direct current magnetron sputtering at room temperature. The width (W) and length (L) of the channel were 750 and 350 μm, respectively.

CQWs Characterization. The ultraviolet–visible absorption spectra were recorded on an Agilent Cary 60 UV–vis Spectrophotometer. Steady-state PL was recorded using a Varian Cary Eclipse at the excitation wavelength of 400 nm. Time-resolved photoluminescence (TRPL) measurement was carried out at excitation wavelength of 375 nm via Horiba JY FL-3. Absolute quantum yield of the CQWs were measured by a commercialized PLQY measurement system from Ocean Optics with a LED excitation source at 400 nm. The XRD patterns were obtained by Panalytical Xpert Pro MPD. HAADF-STEM images and EDS measurements were captured with a FIB-TEM Helios Nanolab 450S. The atomic force microscope measurements were carried out using a digital instrumental multimode nanoscope IIIa in tapping mode.

Device Characterization. UPS spectra were collected on Thermo-VG Scientific ESCALAB 250 Xi equipment with an applied bias of −5 V (data has been corrected by +5 V). A He I ultraviolet radiation source (21.22 eV) was used. The current density–voltage-luminance curve, EL spectra, and EQE measurements of the CQW-LEDs were captured using a XPQY-EQE-350-100 (Guangzhou Xi Pu Optoelectronics Technology Co., Ltd.).

ASSOCIATED CONTENT

Supporting Information

The Supporting Information is available free of charge at https://pubs.acs.org/doi/10.1021/acsnano.2c02967.

Details of the syntheses and characterizations of (CdSe/CdS)@(CdS/CdZnS) ((core/crown)@(c-ALD shell/HIS)) CQWs, electric characteristics of CQW-LEDs and AMCQW-LEDs, and the parameters in device simulation (PDF)

AUTHOR INFORMATION

Corresponding Authors

Baiquan Liu – *State Key Laboratory of Optoelectronic Materials and Technologies, School of Electronics and Information Technology, Sun Yat-sen University, Guangzhou 510275, China;* orcid.org/0000-0001-9375-7683; Email: liubq33@mail.sysu.edu.cn

Jing Wang – *Department of Materials Science and Engineering, City University of Hong Kong, Kowloon, Hong Kong, China*; Email: jingwa3-c@my.cityu.edu.hk

Hilmi Volkan Demir – *UNAM-Institute of Materials Science and Nanotechnology, Department of Electrical and Electronics Engineering, Department of Physics, Bilkent University, Ankara 06800, Turkey; LUMINOUS! Center of Excellence for Semiconductor Lighting and Displays, School of Electrical and Electronic Engineering, School of Physical and Materials Sciences, School of Materials Science and Nanotechnology, Nanyang Technological University,*

https://doi.org/10.1021/acsnano.2c02967
ACS Nano 2022, 16, 10840–10851

Singapore 639798; orcid.org/0000-0003-1793-112X; Email: hvdemir@ntu.edu.sg

Chuan Liu − *State Key Laboratory of Optoelectronic Materials and Technologies, School of Electronics and Information Technology, Sun Yat-sen University, Guangzhou 510275, China*; orcid.org/0000-0002-0695-592X; Email: liuchuan5@mail.sysu.edu.cn

Authors

Sujuan Hu − *State Key Laboratory of Optoelectronic Materials and Technologies, School of Electronics and Information Technology, Sun Yat-sen University, Guangzhou 510275, China*

Farzan Shabani − *UNAM-Institute of Materials Science and Nanotechnology, Department of Electrical and Electronics Engineering, Department of Physics, Bilkent University, Ankara 06800, Turkey*

Lingjiao Zhang − *State Key Laboratory of Optoelectronic Materials and Technologies, School of Electronics and Information Technology, Sun Yat-sen University, Guangzhou 510275, China*

Min Guo − *State Key Laboratory of Optoelectronic Materials and Technologies, School of Electronics and Information Technology, Sun Yat-sen University, Guangzhou 510275, China*

Guanhua Lu − *State Key Laboratory of Optoelectronic Materials and Technologies, School of Electronics and Information Technology, Sun Yat-sen University, Guangzhou 510275, China*

Zhisheng Zhou − *State Key Laboratory of Luminescent Materials and Devices, Institute of Polymer Optoelectronic Materials and Devices, School of Materials Science and Engineering, South China University of Technology, Guangzhou 510640, China*

Jacob C. Huang − *Department of Materials Science and Engineering, City University of Hong Kong, Kowloon, Hong Kong, China; Hong Kong Institute for Advanced Study, City University of Hong Kong, Kowloon, Hong Kong, China*

Yonggang Min − *School of Materials and Energy, Guangdong University of Technology, Guangzhou 510006, China*; orcid.org/0000-0001-9215-8742

Qifan Xue − *State Key Laboratory of Luminescent Materials and Devices, Institute of Polymer Optoelectronic Materials and Devices, School of Materials Science and Engineering, South China University of Technology, Guangzhou 510640, China*; orcid.org/0000-0003-0013-0721

Complete contact information is available at: https://pubs.acs.org/10.1021/acsnano.2c02967

Author Contributions

◆S.H., F.S., and B.L. contributed equally to this work. The manuscript was written through contributions of all authors. All authors have given approval to the final version of the manuscript.

Notes

The authors declare no competing financial interest.

ACKNOWLEDGMENTS

This work was supported in part by National Natural Science Foundation of China under grant nos. 62104265 and 61922090, in part by the Science and Technology Program of Guangdong Province under grant no. 2021A0505110009, and in part by the Innovation and Technology Fund under Grant GHP/006/20GD. J. C. Huang thank the CityU fund (no. 9380088). Y.M. acknowledges the support from the National Natural Science Foundation of China (no. U20A20340), National Key Research and Development Program of China (no. 2020YFB0408100) and Guangdong Innovative and Entrepreneurial Research Team Program (no. 2016ZT06C412). Q.X. acknowledges support from Guangdong Basic and Applied Basic Research Foundation for Distinguished Young Scholar (no. 2021B1515020028) and the Science and Technology Program of Guangzhou, China (no. 201904010147). H.V.D. gratefully acknowledges financial support in part from Agency for Science, Technology and Research (A*STAR) MTC program, grant no. M21J9b0085 (Singapore), Ministry of Education Tier 1 grant MOE-RG62/20 (Singapore) and TUBITAK 115F297, 117E713, 119N343, 121N395, and 20AG001, and support from TUBA.

REFERENCES

(1) Ithurria, S.; Tessier, M. D.; Mahler, B.; Lobo, R. P.; Dubertret, B.; Efros, A. L. Colloidal Nanoplatelets with Two-Dimensional Electronic Structure. *Nat. Mater.* **2011**, *10*, 936−941.

(2) Olutas, M.; Guzelturk, B.; Kelestemur, Y.; Yeltik, A.; Delikanli, S.; Demir, H. V. Lateral Size-Dependent Spontaneous and Stimulated Emission Properties in Colloidal CdSe Nanoplatelets. *ACS Nano* **2015**, *9*, 5041−5050.

(3) Rowland, C. E.; Fedin, I.; Zhang, H.; Gray, S. K.; Govorov, A. O.; Talapin, D. V.; Schaller, R. D. Picosecond Energy Transfer and Multiexciton Transfer Outpaces Auger Recombination in Binary CdSe Nanoplatelet Solids. *Nat. Mater.* **2015**, *14*, 484−489.

(4) Riedinger, A.; Ott, F. D.; Mule, A.; Mazzotti, S.; Knusel, P. N.; Kress, S. J. P.; Prins, F.; Erwin, S. C.; Norris, D. J. An Intrinsic Growth Instability in Isotropic Materials Leads to Quasi-Two-Dimensional Nanoplatelets. *Nat. Mater.* **2017**, *16*, 743−748.

(5) Diroll, B. T.; Chen, M.; Coropceanu, I.; Williams, K. R.; Talapin, D. V.; Guyot-Sionnest, P.; Schaller, R. D. Polarized Near-Infrared Intersubband Absorptions in CdSe Colloidal Quantum Wells. *Nat. Commun.* **2019**, *10*, 4511.

(6) Shornikova, E. V.; Golovatenko, A. A.; Yakovlev, D. R.; Rodina, A. V.; Biadala, L.; Qiang, G.; Kuntzmann, A.; Nasilowski, M.; Dubertret, B.; Polovitsyn, A.; Moreels, I.; Bayer, M. Surface Spin Magnetism Controls the Polarized Exciton Emission from CdSe Nanoplatelets. *Nat. Nanotechnol.* **2020**, *15*, 277−282.

(7) Park, K. H.; Jang, K.; Son, S. U. Synthesis, Optical Properties, and Self-Assembly of Ultrathin Hexagonal In_2S_3 Nanoplates. *Angew. Chem., Int. Ed.* **2006**, *45*, 4608.

(8) Ithurria, S.; Dubertret, B. Quasi 2D Colloidal CdSe Platelets with Thicknesses Controlled at the Atomic Level. *J. Am. Chem. Soc.* **2008**, *130*, 16504−16505.

(9) Salzmann, B. B. V.; Vliem, J. F.; Maaskant, D. N.; Post, L. C.; Li, C.; Bals, S.; Vanmaekelbergh, D. From CdSe Nanoplatelets to Quantum Rings by Thermochemical Edge Reconfiguration. *Chem. Mater.* **2021**, *33*, 6853−6859.

(10) Christodoulou, S.; Climente, J. I.; Planelles, J.; Brescia, R.; Prato, M.; Martin-Garcia, B.; Khan, A. H.; Moreels, I. Chloride-Induced Thickness Control in CdSe Nanoplatelets. *Nano Lett.* **2018**, *18*, 6248−6254.

(11) Mitrofanov, A.; Prudnikau, A.; Di Stasio, F.; Weiß, N.; Hübner, R.; Dominic, A. M.; Borchert, K. B. L.; Lesnyak, V.; Eychmüller, A. Near-Infrared-Emitting $Cd_xHg_{1-x}Se$-Based Core/Shell Nanoplatelets. *Chem. Mater.* **2021**, *33*, 7693−7702.

(12) Yu, J.; Chen, R. Optical Properties and Applications of Two-Dimensional CdSe Nanoplatelets. *InfoMat* **2020**, *2*, 905−927.

(13) Chen, Z.; Nadal, B.; Mahler, B.; Aubin, H.; Dubertret, B. Quasi-2D Colloidal Semiconductor Nanoplatelets for Narrow Electroluminescence. *Adv. Funct. Mater.* **2014**, *24*, 295−302.

(14) Grim, J. Q.; Christodoulou, S.; Di Stasio, F.; Krahne, R.; Cingolani, R.; Manna, L.; Moreels, I. Continuous-Wave Biexciton Lasing at Room Temperature Using Solution-Processed Quantum Wells. *Nat. Nanotechnol.* **2014**, *9*, 891−895.
(15) Sharma, M.; Gungor, K.; Yeltik, A.; Olutas, M.; Guzelturk, B.; Kelestemur, Y.; Erdem, T.; Delikanli, S.; McBride, J. R.; Demir, H. V. Near-Unity Emitting Copper-Doped Colloidal Semiconductor Quantum Wells for Luminescent Solar Concentrators. *Adv. Mater.* **2017**, *29*, 1700821.
(16) Kim, S.; Kim, J. A.; Kim, T.; Chung, H.; Park, S.; Choi, S. M.; Kim, H.-M.; Chung, D.-Y.; Jang, E. Efficient Blue-Light-Emitting Cd-Free Colloidal Quantum Well and Its Application in Electroluminescent Devices. *Chem. Mater.* **2020**, *32*, 5200−5207.
(17) Xiao, P.; Huang, J.; Yan, D.; Luo, D.; Yuan, J.; Liu, B.; Liang, D. Emergence of Nanoplatelet Light-Emitting Diodes. *Materials* **2018**, *11*, 1376.
(18) Kelestemur, Y.; Shynkarenko, Y.; Anni, M.; Yakunin, S.; De Giorgi, M. L.; Kovalenko, M. V. Colloidal CdSe Quantum Wells with Graded Shell Composition for Low-Threshold Amplified Spontaneous Emission and Highly Efficient Electroluminescence. *ACS Nano* **2019**, *13*, 13899−13909.
(19) Qu, J.; Rastogi, P.; Greboval, C.; Livache, C.; Dufour, M.; Chu, A.; Chee, S. S.; Ramade, J.; Xu, X. Z.; Ithurria, S.; Lhuillier, E. Nanoplatelet-Based Light-Emitting Diode and Its Use in All-Nanocrystal LiFi-like Communication. *ACS Appl. Mater. Interfaces* **2020**, *12*, 22058−22065.
(20) Tessier, M. D.; Spinicelli, P.; Dupont, D.; Patriarche, G.; Ithurria, S.; Dubertret, B. Efficient Exciton Concentrators Built from Colloidal Core/Crown CdSe/CdS Semiconductor Nanoplatelets. *Nano Lett.* **2014**, *14*, 207−213.
(21) Shabani, F.; Dehghanpour Baruj, H.; Yurdakul, I.; Delikanli, S.; Gheshlaghi, N.; Isik, F.; Liu, B.; Altintas, Y.; Canimkurbey, B.; Demir, H. V. Deep-Red-Emitting Colloidal Quantum Well Light-Emitting Diodes Enabled through a Complex Design of Core/Crown/Double Shell Heterostructure. *Small* **2022**, *18*, 2106115.
(22) Jing, L.; Kershaw, S. V.; Li, Y.; Huang, X.; Li, Y.; Rogach, A. L.; Gao, M. Aqueous Based Semiconductor Nanocrystals. *Chem. Rev.* **2016**, *116*, 10623−10730.
(23) Altintas, Y.; Liu, B.; Hernández-Martínez, P. L.; Gheshlaghi, N.; Shabani, F.; Sharma, M.; Wang, L.; Sun, H.; Mutlugun, E.; Demir, H. V. Spectrally Wide-Range-Tunable, Efficient, and Bright Colloidal Light-Emitting Diodes of Quasi-2D Nanoplatelets Enabled by Engineered Alloyed Heterostructures. *Chem. Mater.* **2020**, *32*, 7874−7883.
(24) Peric, N.; Lambert, Y.; Singh, S.; Khan, A. H.; Franchina Vergel, N. A.; Deresmes, D.; Berthe, M.; Hens, Z.; Moreels, I.; Delerue, C.; Grandidier, B.; Biadala, L. Van Hove Singularities and Trap States in Two-Dimensional CdSe Nanoplatelets. *Nano Lett.* **2021**, *21*, 1702−1708.
(25) Dutta, A.; Medda, A.; Patra, A. Recent Advances and Perspectives on Colloidal Semiconductor Nanoplatelets for Optoelectronic Applications. *J. Phys. Chem. C* **2021**, *125*, 20−30.
(26) Fan, F.; Kanjanaboos, P.; Saravanapavanantham, M.; Beauregard, E.; Ingram, G.; Yassitepe, E.; Adachi, M. M.; Voznyy, O.; Johnston, A. K.; Walters, G.; Kim, G. H.; Lu, Z. H.; Sargent, E. H. Colloidal $CdSe_{1-x}S_x$ Nanoplatelets with Narrow and Continuously-Tunable Electroluminescence. *Nano Lett.* **2015**, *15*, 4611−4615.
(27) Giovanella, U.; Pasini, M.; Lorenzon, M.; Galeotti, F.; Lucchi, C.; Meinardi, F.; Luzzati, S.; Dubertret, B.; Brovelli, S. Efficient Solution-Processed Nanoplatelet-Based Light-Emitting Diodes with High Operational Stability in Air. *Nano Lett.* **2018**, *18*, 3441−3448.
(28) Dufour, M.; Qu, J.; Greboval, C.; Methivier, C.; Lhuillier, E.; Ithurria, S. Halide Ligands to Release Strain in Cadmium Chalcogenide Nanoplatelets and Achieve High Brightness. *ACS Nano* **2019**, *13*, 5326−5334.
(29) Liu, B.; Delikanli, S.; Gao, Y.; Dede, D.; Gungor, K.; Demir, H. V. Nanocrystal Light-Emitting Diodes Based on Type II Nanoplatelets. *Nano Energy* **2018**, *47*, 115−122.
(30) Liu, B.; Sharma, M.; Yu, J.; Shendre, S.; Hettiarachchi, C.; Sharma, A.; Yeltik, A.; Wang, L.; Sun, H.; Dang, C.; Demir, H. V. Light-Emitting Diodes with Cu-Doped Colloidal Quantum Wells: From Ultrapure Green, Tunable Dual-Emission to White Light. *Small* **2019**, *15*, 1901983.
(31) Liu, B.; Altintas, Y.; Wang, L.; Shendre, S.; Sharma, M.; Sun, H.; Mutlugun, E.; Demir, H. V. Record High External Quantum Efficiency of 19.2% Achieved in Light-Emitting Diodes of Colloidal Quantum Wells Enabled by Hot-Injection Shell Growth. *Adv. Mater.* **2020**, *32*, 1905824.
(32) Lin, K.; Xing, J.; Quan, L. N.; De Arquer, F. P. G.; Gong, X.; Lu, J.; Xie, L.; Zhao, W.; Zhang, D.; Yan, C.; Li, W.; Liu, X.; Lu, Y.; Kirman, J.; Sargent, E. H.; Xiong, Q.; Wei, Z. Perovskite Light-Emitting Diodes with External Quantum Efficiency Exceeding 20%. *Nature* **2018**, *562*, 245−248.
(33) Cao, Y.; Wang, N.; Tian, H.; Guo, J.; Wei, Y.; Chen, H.; Miao, Y.; Zou, W.; Pan, K.; He, Y.; Cao, H.; Ke, Y.; Xu, M.; Wang, Y.; Yang, M.; Du, K.; Fu, Z.; Kong, D.; Dai, D.; Jin, Y.; Li, G.; Li, H.; Peng, Q.; Wang, J.; Huang, W. Perovskite Light-Emitting Diodes Based on Spontaneously Formed Submicrometre-Scale Structures. *Nature* **2018**, *562*, 249−253.
(34) Li, X.; Zhao, Y.-B.; Fan, F.; Levina, L.; Liu, M.; Quintero-Bermudez, R.; Gong, X.; Quan, L. N.; Fan, J.; Yang, Z.; Hoogland, S.; Voznyy, O.; Lu, Z.-H.; Sargent, E. H. Bright Colloidal Quantum Dot Light-Emitting Diodes Enabled by Efficient Chlorination. *Nat. Photonics.* **2018**, *12*, 159−164.
(35) Shen, X.; Zhang, Y.; Kershaw, S. V.; Li, T.; Wang, C.; Zhang, X.; Wang, W.; Li, D.; Wang, Y.; Lu, M.; Zhang, L.; Sun, C.; Zhao, D.; Qin, G.; Bai, X.; Yu, W. W.; Rogach, A. L. Zn-Alloyed $CsPbI_3$ Nanocrystals for Highly Efficient Perovskite Light-Emitting Devices. *Nano Lett.* **2019**, *19*, 1552−1559.
(36) Vasilopoulou, M.; Kim, H. P.; Kim, B. S.; Papadakis, M.; Ximim Gavim, A. E.; Macedo, A. G.; Jose da Silva, W.; Schneider, F. K.; Mat Teridi, M. A.; Coutsolelos, A. G.; bin Mohd Yusoff, A. R. Efficient Colloidal Quantum Dot Light-Emitting Diodes Operating in the Second Near-Infrared Biological Window. *Nat. Photonics.* **2020**, *14*, 50−56.
(37) Liu, Z.; Qiu, W.; Peng, X.; Sun, G.; Liu, X.; Liu, D.; Li, Z.; He, F.; Shen, C.; Gu, Q.; Ma, F.; Yip, H. L.; Hou, L.; Qi, Z.; Su, S. J. Perovskite Light-Emitting Diodes with EQE Exceeding 28% through a Synergetic Dual-Additive Strategy for Defect Passivation and Nanostructure Regulation. *Adv. Mater.* **2021**, *33*, 2103268.
(38) Liu, X. K.; Xu, W.; Bai, S.; Jin, Y.; Wang, J.; Friend, R. H.; Gao, F. Metal Halide Perovskites for Light-Emitting Diodes. *Nat. Mater.* **2021**, *20*, 10−21.
(39) Liu, M.; Yazdani, N.; Yarema, M.; Jansen, M.; Wood, V.; Sargent, E. H. Colloidal Quantum Dot Electronics. *Nat. Electron.* **2021**, *4*, 548−558.
(40) Miao, Y.; Liu, X.; Chen, Y.; Zhang, T.; Wang, T.; Zhao, Y. Deep-Red Perovskite Light-Emitting Diodes Based on One-Step-Formed gamma-$CsPbI_3$ Cuboid Crystallites. *Adv. Mater.* **2021**, *33*, 2105699.
(41) Zou, W.; Li, R.; Zhang, S.; Liu, Y.; Wang, N.; Cao, Y.; Miao, Y.; Xu, M.; Guo, Q.; Di, D.; et al. Minimising Efficiency Roll-Off in High-Brightness Perovskite Light-Emitting Diodes. *Nat. Commun.* **2018**, *9*, 608.
(42) Lin, Q.; Song, B.; Wang, H.; Zhang, F.; Chen, F.; Wang, L.; Li, L. S.; Guo, F.; Shen, H. High-Efficiency Deep-Red Quantum-Dot Light-Emitting Diodes with Type-II CdSe/CdTe Core/Shell Quantum Dots as Emissive Layers. *J. Mater. Chem. C* **2016**, *4*, 7223−7229.
(43) Pan, J.; Shang, Y.; Yin, J.; De Bastiani, M.; Peng, W.; Dursun, I.; Sinatra, L.; El-Zohry, A. M.; Hedhili, M. N.; Emwas, A. H.; Mohammed, O. F.; Ning, Z.; Bakr, O. M. Bidentate Ligand-Passivated $CsPbI_3$ Perovskite Nanocrystals for Stable Near-Unity Photoluminescence Quantum Yield and Efficient Red Light-Emitting Diodes. *J. Am. Chem. Soc.* **2018**, *140*, 562−565.
(44) Kathirgamanathan, P.; Kumaraverl, M.; Bramananthan, N.; Ravichandran, S. High Efficiency and Highly Saturated Red Emitting

https://doi.org/10.1021/acsnano.2c02967
ACS Nano 2022, 16, 10840−10851

Inverted Quantum Dot Devices (QLEDs): Optimisation of Their Efficiencies with Low Temperature Annealed Sol−Gel Derived ZnO as the Electron Transporter and A Novel High Mobility Hole Transporter and Thermal Annealing of the Devices. *J. Mater. Chem. C* **2018**, *6*, 11622−11644.
(45) He, J. L.; Kong, F. C.; Sun, B.; Wang, X. J.; Tian, Q. S.; Fan, J.; Liao, L. S. Highly Efficient Deep-Red TADF Organic Light-Emitting Diodes via Increasing the Acceptor Strength of Fused Polycyclic Aromatics. *Chem. Eng. J.* **2021**, *424*, 130470.
(46) Ithurria, S.; Talapin, D. V. Colloidal Atomic Layer Deposition (c-ALD) Using Self-Limiting Reactions at Nanocrystal Surface Coupled to Phase Transfer between Polar and Nonpolar Media. *J. Am. Chem. Soc.* **2012**, *134*, 18585−18590.
(47) Dai, X.; Zhang, Z.; Jin, Y.; Niu, Y.; Cao, H.; Liang, X.; Chen, L.; Wang, J.; Peng, X. Solution-Processed, High-Performance Light-Emitting Diodes Based on Quantum Dots. *Nature* **2014**, *515*, 96−99.
(48) Zhang, Z.; Ye, Y.; Pu, C.; Deng, Y.; Dai, X.; Chen, X.; Chen, D.; Zheng, X.; Gao, Y.; Fang, W.; Peng, X.; Jin, Y. High-Performance, Solution-Processed, and Insulating-Layer-Free Light-Emitting Diodes Based on Colloidal Quantum Dots. *Adv. Mater.* **2018**, *30*, 1801387.
(49) Moon, H.; Lee, W.; Kim, J.; Lee, D.; Cha, S.; Shin, S.; Chae, H. Composition-Tailored ZnMgO Nanoparticles for Electron Transport Layers of Highly Efficient and Bright InP-based Quantum Dot Light Emitting Diodes. *Chem. Commun.* **2019**, *55*, 13299−13302.
(50) Zhu, R.; Luo, Z.; Chen, H.; Dong, Y.; Wu, S. T. Realizing Rec. 2020 Color Gamut with Quantum Dot Displays. *Opt. Express.* **2015**, *23*, 23680−23693.
(51) Baldo, M. A.; Adachi, C.; Forrest, S. R. Transient Analysis of Organic Electrophosphorescence. II. Transient Analysis of Triplet-Triplet Annihilation. *Phys. Rev. B* **2000**, *62*, 10967.
(52) Liu, A.; Liu, G. X.; Zhu, H. H.; Xu, F.; Fortunato, E.; Martins, R.; Shan, F. K. Fully Solution-Processed Low-Voltage Aqueous In_2O_3 Thin-Film Transistors Using an Ultrathin ZrO_x Dielectric. *ACS Appl. Mater. Interfaces* **2014**, *6*, 17364−17369.
(53) Krausmann, J.; Sanctis, S.; Engstler, J.; Luysberg, M.; Bruns, M.; Schneider, J. J. Charge Transport in Low-Temperature Processed Thin-Film Transistors Based on Indium Oxide/Zinc Oxide Heterostructures. *ACS Appl. Mater. Interfaces* **2018**, *10*, 20661−20671.
(54) Liu, B. Q.; Wang, L.; Gao, D. Y.; Zou, J. H.; Ning, H. L.; Peng, J. B.; Cao, Y. Extremely High-Efficiency and Ultrasimplified Hybrid White Organic Light-Emitting Diodes Exploiting Double Multifunctional Blue Emitting Layers. *Light Sci. Appl.* **2016**, *5*, No. e16137.
(55) He, P.; Jiang, C.; Lan, L.; Sun, S.; Li, Y.; Gao, P.; Zhang, P.; Dai, X.; Wang, J.; Peng, J.; Cao, Y. High-Performance, Solution-Processed Quantum Dot Light-Emitting Field-Effect Transistors with a Scandium-Incorporated Indium Oxide Semiconductor. *ACS Nano* **2018**, *12*, 4624−4629.
(56) Choi, M.; Bae, S. R.; Hu, L.; Hoang, A. T.; Kim, S. Y.; Ahn, J. H. Full-Color Active-Matrix Organic Light-Emitting Diode Display on Human Skin Based on a Large-Area MoS_2 Backplane. *Sci. Adv.* **2020**, *6*, No. eabb5898.
(57) Sekitani, T.; Nakajima, H.; Maeda, H.; Fukushima, T.; Aida, T.; Hata, K.; Someya, T. Stretchable Active-Matrix Organic Light-Emitting Diode Display Using Printable Elastic Conductors. *Nat. Mater.* **2009**, *8*, 494−499.
(58) Kim, T. H.; Cho, K. S.; Lee, E. K.; Lee, S. J.; Chae, J.; Kim, J. W.; Kim, D. H.; Kwon, J. Y.; Amaratunga, G.; Lee, S. Y.; Choi, B. L.; Kuk, Y.; Kim, J. M.; Kim, K. Full-Colour Quantum Dot Displays Fabricated by Transfer Printing. *Nat. Photonics.* **2011**, *5*, 176−182.
(59) Kwon, G.; Kim, K.; Choi, B. D.; Roh, J.; Lee, C.; Noh, Y. Y.; Seo, S.; Kim, M. G.; Kim, C. Multifunctional Organic-Semiconductor Interfacial Layers for Solution-Processed Oxide-Semiconductor Thin-Film Transistor. *Adv. Mater.* **2017**, *29*, 1607055.
(60) Chen, C.; Chen, Z.; Xu, K.; Zheng, J.; Ou, H.; Wang, Z.; Chen, H.; Liu, X.; Wu, Q.; Chan, P. K. L.; Liu, C. Thin-Film Transistors with the Fringe Effect and the Correction Factor for Mobility Extraction. *IEEE Electron Device Lett.* **2019**, *40*, 897−900.
(61) Liu, C.; Li, X.; Luo, Y.; Wang, Y.; Hu, S.; Liu, C.; Liang, X.; Zhou, H.; Chen, J.; She, J.; Deng, S. How Materials and Device Factors Determine the Performance: A Unified Solution for Transistors with Nontrivial Gates and Transistor-Diode Hybrid Integration. *Adv. Sci.* **2022**, *9*, 2104896.
(62) Zhang, Z.; Ye, Y.; Pu, C.; Deng, Y.; Dai, X.; Chen, X.; Chen, X.; Chen, D.; Zheng, X.; Gao, Y.; et al. High-Performance, Solution-Processed, and Insulating-Layer-Free Light-Emitting Diodes Based on Colloidal Quantum Dots. *Adv. Mater.* **2018**, *30*, 1801387.

https://doi.org/10.1021/acsnano.2c02967
ACS Nano 2022, 16, 10840−10851